Applied Catalysis B: Environmental 322 (2023) 122135

Contents lists available at ScienceDirect

Applied Catalysis B: Environmental

journal homepage: www.elsevier.com/locate/apcatb

Linker length-dependent photocatalytic activity of β-ketoenamine covalent organic frameworks

Kanghui Xiong, Yuexin Wang, Fulin Zhang, Xia Li, Xianjun Lang *

Sauvage Center for Molecular Sciences and Hubei Key Lab on Organic and Polymeric Optoelectronic Materials, College of Chemistry and Molecular Sciences, Wuhan University, Wuhan 430072, China

ARTICLE INFO

Keywords:
Photocatalysis
Covalent organic frameworks
β-Ketoenamine
Selective oxidation

ABSTRACT

Myriad endeavors have shifted towards covalent organic frameworks (COFs) for their aptitude in visible light photocatalysis. Herein, three β-ketoenamine COFs with different linker lengths, i.e., TpPa-COF, TpBD-COF, and TpDT-COF, were synthesized from 1,3,5-triformylphloroglucinol and 1,4-benzenediamine, 4,4'-biphenyldiamine, and 4,4''-*p*-terphenyldiamine, respectively. With the shortest linker, a noticeable conversion of benzylamine was observed by TpPa-COF photocatalysis. By prolonging the linker length, TpBD-COF performed a better conversion of benzylamine, which might be due to more suitable redox potentials than TpPa-COF. However, with the longest linker, TpDT-COF resulted in a lower conversion than TpBD-COF, which might be ascribed to the slightly inferior optoelectronic properties. With a moderate linker length, TpBD-COF convincingly delivered the best photocatalytic activity for the violet light-driven aerobic oxidation of amines. This work sheds light on the dimension of linker length in designing more active COF photocatalysts.

1. Introduction

As novel crystalline porous materials, covalent organic frameworks (COFs) are built out of light elements that are held together by covalent bonds [1–3]. Due to their unique properties, such as outstanding flexibility, permanent porosity, and ordered structures, COFs have drawn tremendous attention [4–6]. As such, COFs have found applications in energy storage [7–9], gas storage and separation [10–14], optoelectronics [15,16], and catalysis [17–19]. Because of the high crystallinity and extended π-conjugation, COFs have recently been defined as one of the most auspicious materials [20–22]. In addition, COFs have attracted myriad endeavors to explore their photocatalytic aptitudes [23–26]. Moreover, the high crystallinity and π–π stacking interaction provide applicable channels for charge carriers [27] and effectively reduce undesired defects for charge trapping [28]. These attributes are conducive to promoting their photocatalytic activity for copious reactions [29,30].

The diversity of building blocks and reversible covalent bonds endow COFs with designable crystalline structures [31–33]. Numerous well-designed COFs with specific topologies, pore sizes, and bespoke functions have been synthesized by choosing different building blocks [34–37]. However, controlling the linker length to precisely manipulate the property of COFs for improving their photocatalytic activity is scarcely reported. A new dimension of renovation is opening up on this front.

The β-ketoenamine bonds have been extensively used to build 2D COF photocatalysts [38–40]. Because of the built-in characteristics, β-ketoenamine COFs possess not only good crystallinity and tunable porosity [41–43] but also favorable electronic structures [44–46], leading to exceptional activity in visible light photocatalysis [47–49]. In addition, it is valuable to explore the intrinsic structure–activity relationship of β-ketoenamine COFs. So that, there is plenty of space for the rational design of β-ketoenamine COFs to develop state-of-the-art photocatalysts.

Herein, three β-ketoenamine COFs with different linker lengths, i.e., TpPa-COF, TpBD-COF, and TpDT-COF, were built out of 1,3,5-triformylphloroglucinol and 1,4-benzenediamine, 4,4'-biphenyldiamine, and 4,4''-*p*-terphenyldiamine, respectively. The three β-ketoenamine COFs had similar chemical structures yet varying linker lengths. Furthermore, the crystallinity, morphologies, and properties of the three COFs were systematically characterized. In appearance, TpPa-COF, TpBD-COF, and TpDT-COF exhibited dark red to orange color which might be due to the discrepancy of the extensive π-conjugations. In depth, the redox potentials of the three COFs shifted, in particular from TpPa-COF to TpBD-COF, by varying the linker lengths. Intentionally, the intrinsic

* Corresponding author.
E-mail address: xianjunlang@whu.edu.cn (X. Lang).

https://doi.org/10.1016/j.apcatb.2022.122135
Received 30 September 2022; Received in revised form 24 October 2022; Accepted 30 October 2022
Available online 1 November 2022

structure–activity relationship was explored by the aerobic oxidation of amines to imines. Employing the three COFs as metal-free photocatalysts for the violet light-driven aerobic oxidation of amines to imines, the conversions followed by the sequence of TpBD-COF > TpDT-COF > TpPa-COF. The results showed that the photocatalytic activity of the β-ketoenamine COFs could be tuned the linker lengths towards more favorable oxidation of amines to imines. Finally, a feasible direction of travel has been sketched out for designing COF photocatalysts by varying the linker lengths.

2. Experimental section

2.1. Synthesis of the three β-ketoenamine COFs

With slight modifications, TpPa-COF and TpBD-COF were synthesized according to a prior report [50]. 1,3,5-Triformylphloroglucinol (0.3 mmol) and corresponding diamine (1,4-benzenediamine or 4,4′-biphenyldiamine 0.45 mmol) were charged into a Pyrex tube, and followed by adding 6 M aqueous acetic acid (0.5 mL), dioxane (1.5 mL) and mesitylene (1.5 mL). After 30 min of ultrasonication at room temperature, the mixture was swiftly frozen in an N_2 liquid bath (77 K) and then sealed under vacuum after three freeze–pump–thaw cycles. The homogenous solution was transferred into an oven and stayed at 120 ℃ for 72 h. The precipitate was obtained by filtering separation and was washed with acetone and tetrahydrofuran three times. Finally, the product was purified by Soxhlet extraction in tetrahydrofuran for 24 h, followed by drying to obtain the corresponding COFs under vacuum at 100 ℃. The synthesis of TpDT-COF was similar to TpPa-COF and TpBD-COF with diamine as 4,4′′-*p*-terphenyldiamine (0.45 mmol) except mesitylene (1.5 mL) was replaced by 1,2-dichlorobenzene (1.5 mL).

2.2. Protocol for selective oxidation of amine

Firstly, benzylamine (0.3 mmol) and TpBD-COF (5 mg) were dispersed in 1 mL acetonitrile (CH_3CN) in a 10 mL Pyrex photoreactor. The resulted mixture was stirred by a magnetic stir bar for 30 min under dark condition. Then, the reaction mixture was stirred at 1500 rpm under air and irradiated by violet LEDs (3 W × 4). After reaction, the mixture was centrifugated to remove the solid components. The conversion (Conv. %) for the substrate and the selectivity (Sel. %) for the product were determined by a gas chromatograph with a flame ionization detector (GC–FID) through an internal standard method. Moreover, the products were also substantiated by gas chromatography–mass spectrometry.

3. Results and discussion

3.1. Design and characterizations of the three COFs with different linker lengths

Firstly, the three β-ketoenamine COFs with different linker lengths were synthesized under solvothermal conditions by reacting 1,3,5-triformylphloroglucinol with their respective diamines, affording TpPa-COF, TpBD-COF, and TpDT-COF (Fig. 1). Then, the chemical structures and properties of the three COFs with different linker lengths were verified by a series of characterizations. Under the same conditions for the synthesis of TpPa-COF and TpBD-COF, TpDT-COF was synthesized with relatively poor crystallinity (Supplementary Fig. S1). Therefore, minor modification of replacing the solvent mesitylene with 1,2-dichlorobenzene was made.

Next, powder X-ray diffraction (PXRD) was utilized to assess the crystallinity of TpPa-COF, TpBD-COF, and TpDT-COF (Fig. 2a). The PXRD pattern of TpPa-COF exhibits an intense peak at 4.8°, corresponding to the (100) plane. And slight peaks also appear at 8.5° and 26.8°. Analogously, the PXRD pattern of TpBD-COF shows three diffraction peaks at 3.6°, 6.0°, and 27.6°, which could be attributed to the (100), (200), and (001) planes, respectively. Besides, the primary diffraction peak of TpDT-COF at 2.8° is indexed as the reflection from the (100) plane, and two peaks at 4.78° and 26.5° are assigned to the reflections from the (200) and (001) planes, respectively. The results comply with the previously reported theoretical prediction of the AA

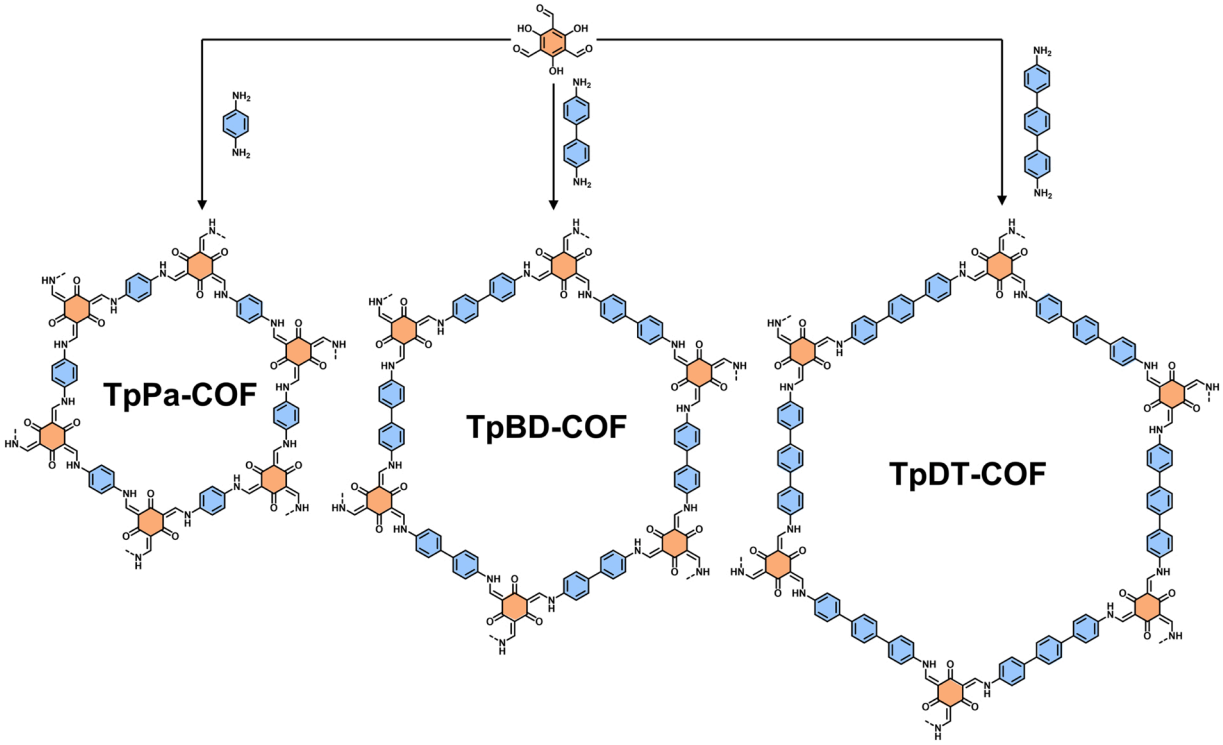

Fig. 1. The design of the three β-ketoenamine COFs with different linker lengths.

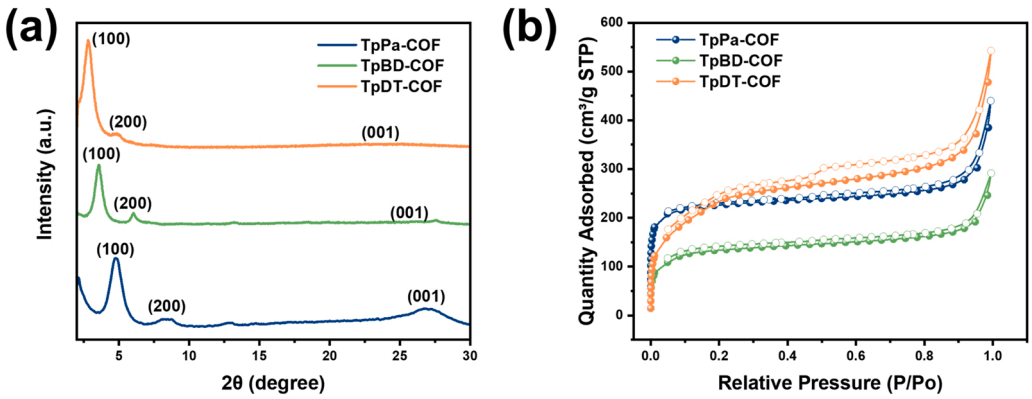

Fig. 2. (a) PXRD patterns and (b) N_2 adsorption/desorption isotherms of the three COFs with different linker lengths.

eclipsed layer stacking model [50,51]. The successful synthesis of the three COFs with different linker lengths was further corroborated by comparison with the PXRD patterns of their corresponding building blocks (Supplementary Fig. S2). Moreover, the PXRD patterns of TpPa-COF, TpBD-COF, and TpDT-COF are slightly different, with the diffraction peaks moving to smaller angles due to the increase of the linker lengths of the building blocks.

The permanent porosities of TpPa-COF, TpBD-COF, and TpDT-COF were investigated by N_2 adsorption/desorption isotherms at 77 K (Fig. 2b). The results in Fig. 2b show steep uptakes of all COFs are reached at lower pressure ($P/P_0 < 0.05$). These correspond to the characteristic type I sorption isotherm, indicating the existence of a wide variety of pores. In detail, the Brunauer–Emmett–Teller (BET) specific surface areas of the three COFs were estimated to be 837, 483, and 871 $m^2\ g^{-1}$, respectively. On the basis of non-local density functional theory (DFT) models (Supplementary Fig. S3), the pore size distributions were estimated to be 1.2, 1.3, and 2.3 nm, respectively. This trend is in good consistency with the linker lengths.

The scanning electron microscopy (SEM) images of the three COFs with different linker lengths disclose their flower-like morphologies. According to the SEM image of TpPa-COF (Fig. 3a), these flower petals contain spike-shaped tips and rod structures. Whereas for TpBD-COF (Fig. 3b) and TpDT-COF (Fig. 3c), the flower petals are expanded much wider into sheet-like structures. These differences could be regarded as the result that COF layers tend to π–π stacking. Interestingly, these differences in morphologies should mainly depend on the effect of linker lengths of the COFs, considering that the synthesis conditions of these COFs were pretty similar. Besides, transmission electron microscopy (TEM) could further characterize the morphologies of the three COFs with different linker lengths. The TEM images reveal that there is the presence of fringes in TpBD-COF, while there are no apparent fringes in both TpPa-COF and TpDT-COF (Supplementary Fig. S4).

Furthermore, the three COFs with different linker lengths were verified by Fourier transform infrared (FTIR) spectroscopy and solid-state ^{13}C cross-polarization magic angle spinning nuclear magnetic resonance (CP-MAS NMR). In the FTIR spectra (Supplementary Fig. S5–7) of the three β-ketoenamine COFs, the peaks at the 3300 cm^{-1} and 1633 cm^{-1} vanish, representing the disappearance of N—H stretching peak and the aldehyde stretching peak in their corresponding building blocks, respectively. Meanwhile, the presence of the C═O stretching peak at 1587 cm^{-1} and the C═C stretching peak at 1610 cm^{-1} confirms the condensation between amines and aldehydes and the formation of enol to keto tautomerism [52]. According to solid-state ^{13}C CP-MAS NMR spectra (Supplementary Fig. S8), the three β-ketoenamine COFs exhibit a clear signal around 185 ppm, arising from the carbonyl carbons. Two peaks around 147 ppm and 107 ppm are attributed to carbons of C═C, which further certifies the formation of enol to keto tautomerism [53]. Additionally, the thermal stabilities of the three COFs with different linker lengths were characterized by thermogravimetric analysis (TGA) (Supplementary Fig. S9) under an atmosphere of nitrogen. The onset temperatures of decomposition for TpPa-COF, TpBD-COF, and TpDT-COF are 400, 350, and 420 ℃, respectively.

Next, there was a systematic investigation of the three COFs with different linker lengths by ultraviolet–visible diffuse reflectance spectroscopy (UV–vis DRS) and the corresponding Mott–Schottky plots. As shown in Fig. 4a, it appears clearly that the absorption profiles of the three COFs are in the range of 200–550 nm, indicating the strong absorption to visible light. The hypsochromic shift of absorption band appear evidently with increasing the lengths of aromatic diamine linkers. In addition, their corresponding bandgaps were calculated to be 2.12 eV for TpPa-COF, 2.25 eV for TpBD-COF, and 2.30 eV for TpDT-COF based on Kubelka–Munk equation (Fig. 4b). This elucidates that the increase of the linker lengths in the COFs would broaden the optical bandgaps. Besides, Mott–Schottky tests could figure out the type of conductivity. Each of the curves in Mott–Schottky tests are a positive slope (Supplementary Fig. S10–12), which suggests that all the three COFs are typical n-type semiconductors [54]. Meanwhile, based on Mott–Schottky analysis identified from the intersection points, the lowest unoccupied molecular orbital (LUMO) levels of the three COFs were estimated to be −1.03, −0.86, and −0.85 V versus Ag/AgCl, respectively. Combined with the bandgaps, the corresponding highest

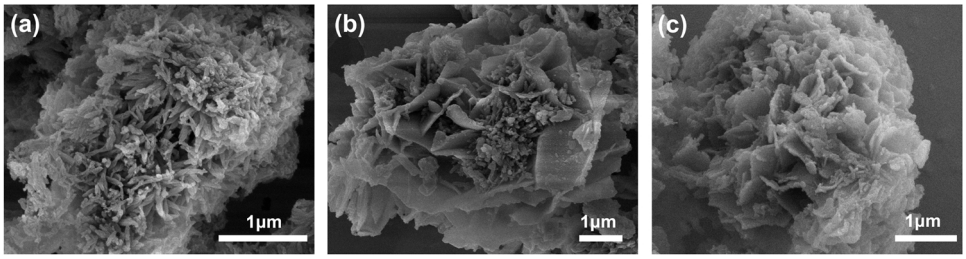

Fig. 3. SEM images of (a) TpPa-COF, (b) TpBD-COF, and (c) TpDT-COF.

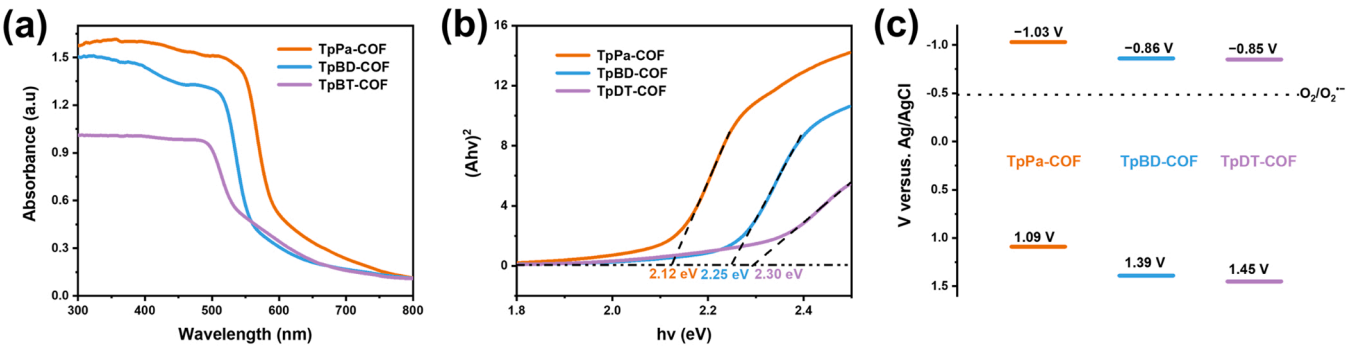

Fig. 4. (a) The UV–vis DRS, (b) the corresponding Tauc plot analysis, and (c) the calculated band structures of the three β-ketoenamine COFs.

occupied molecular orbital (HOMO) levels of TpPa-COF, TpBD-COF and TpDT-COF were estimated to be +1.09, +1.39, and +1.45 V versus Ag/AgCl, respectively. Accordingly, the band structures of the three COFs were exhibited in Fig. 4c. In consideration of the band structures, the three COFs with different linker lengths were capable of activating O_2 to superoxide anion radical ($O_2^{\bullet-}$). Moreover, the photocurrent intensity could be used to evaluated the electron transfer efficiency (Fig. 5a), and the electrochemical impedance spectroscopy (EIS) could be used to assess the internal resistance for the charge transfer (Fig. 5b). To a large extent, the photocurrent intensity and the semicircle diameter did not vary with the linker length as expected. Notably, TpBD-COF with a moderate linker length showed better charge separation and transfer and lower resistance.

3.2. Aerobic oxidation of amines by COF photocatalysis

Hitherto, some COF photocatalysts have exhibited aptitude in the selective formation of covalent bonds [55–57], which in turn is opportune to underscore both the covalent bonds and the linkers. In particular, the photocatalytic aerobic oxidation of amines to imines is highly important in organic transformations [58–61]. There are notable reports for the photocatalytic formation of imines over imine COFs [62,63]. However, the reversible imine bonds of these COFs are susceptible to the attack of substrate benzyl amines. Therefore, for the oxidation of benzyl amines, COFs held together by less reversible covalent bonds like olefins [64,65] and β-ketoenamines [66–68] would seem more apropos. The effect of the linker lengths on photocatalytic activity of the three β-ketoenamine COFs was elucidated with the selective aerobic oxidation of benzylamine. First the solvent was screened in ethanol (C_2H_5OH), methanol (CH_3OH), and CH_3CN (Supplementary Table S1). With the best conversion, CH_3CN was selected as the solvent. Then, experiments were applied to compare the three COFs with different linker lengths in photocatalytic activity. The results in Fig. 6a demonstrate that TpBD-COF manifestly exhibited the highest conversion amongst the three β-ketoenamine COFs. In detail, 78% conversion of benzylamine was obtained by TpBD-COF photocatalysis, whereas 22% conversion over TpPa-COF and 61% conversion over TpDT-COF were reaped under the same conditions. According to the kinetic plots (Fig. 6b), reactions over all the three COFs with different linker lengths were in accord with zero-order kinetics. Evidently the highest conversion rate of benzylamine over TpBD-COF was further proved. Therefore, TpBD-COF, the best photocatalyst, was picked for the following investigations. Then, factors affecting the photocatalytic activity for selective oxidation of benzylamine were studied. Clearly, the reaction almost stopped in the absence of TpBD-COF, light irradiation, or air, which indicates all of these factors played an indispensable role (Supplementary Table S2). In addition, the photocatalytic activity of the building blocks was verified (Supplementary Table S3). There were almost no conversions of benzylamine in the presence of diamine alone. In contrast, there was 20% conversion of benzylamine in the presence of 1,3,5-triformylphloroglucinol irradiated by violet LEDs.

Considering the broad absorption in the visible region, the effect of LEDs of different peak wavelengths (λ_p) was studied (Fig. 7a). The trend of conversions of benzylamine irradiated by different LEDs shows that a decrease in the λ_p of LEDs results in the increase of the conversions of benzylamine, which is in excellent accordance with the UV–vis DRS of TpBD-COF. Accordingly, violet LEDs (the light-emitting spectrum, Supplementary Fig. S13) were selected as the light source in the subsequent reactions for the selective oxidation of amines due to the best efficiency. Besides, it is pivotal to maintain recyclability in long-term photocatalytic reactions. The results of recycling experiment was plotted in Fig. 7b. TpBD-COF preserved most of the conversions of benzylamine after three photocatalytic cycles, indicating the excellent durability and recyclability of TpBD-COF. The slight decline in the conversions could be attributed to the inevitable loss of TpBD-COF during recycling.

Subsequently, for superior computational cost effectiveness, the bandgaps of the three COFs of the the optimized fragment structures

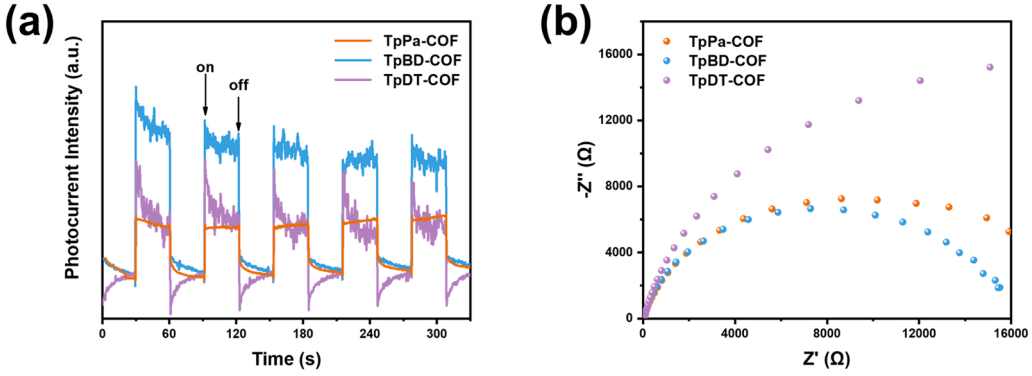

Fig. 5. (a) Transient photocurrents and (b) EIS of the three β-ketoenamine COFs.

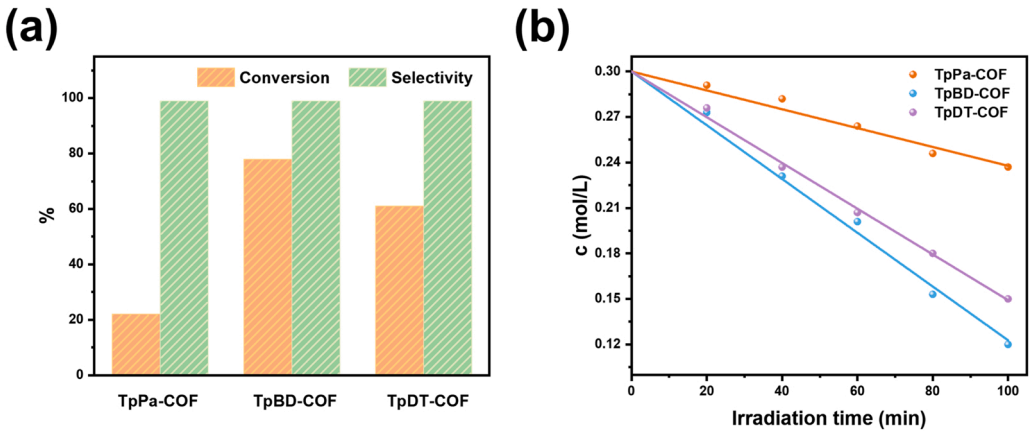

Fig. 6. Comparison of (a) conversions and (b) kinetic plots for the selective aerobic oxidation of benzylamine by TpPa-COF, TpBD-COF, and TpDT-COF photocatalysis. Reaction conditions: photocatalyst (5 mg), benzylamine (0.3 mmol), violet LEDs, CH_3CN (1 mL), air (1 atm), 2 h.

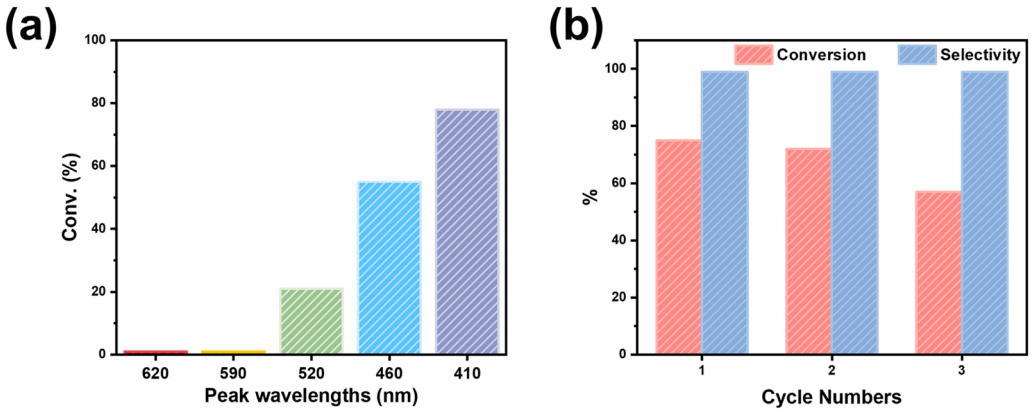

Fig. 7. (a) The selective oxidation of benzylamine by TpBD-COF photocatalysis irradiated by LEDs of different λ_p; (b) The recyclability of TpBD-COF photocatalyst for the selective oxidation of benzylamine. Reaction conditions: TpBD-COF (5 mg), benzylamine (0.3 mmol), violet LEDs, CH_3CN (1 mL), air (1 atm), 2 h.

were calculated (Supplementary Table S4) from DFT at B3LYP/6-31G(d, p) level. Coinciding well with the optical bandgaps calculated from UV–vis DRS, the bandgaps of the three COFs increased with the length linker increase as well. Besides, it could be revealed that all of the atoms of TpPa-COF are coplanar and linkers of TpBD-COF and TpDT-COF rotate out of the plane in their optimized structures with electrostatic potential (ESP) surface maps (Fig. 8). So that, the increases of the bandgaps could also be ascribed that planarity and conjugation of the COFs fade caused by the composite effect of the Cortho's energy behavior and steric clash of destabilization in two *ortho*-hydrogens [69, 70]. This could be used to make clear that TpBD-COF has better absorption to violet light compared to red and green light. As depicted in Fig. 8, ESP maps demonstrate that negative potential focus on the O atom of the carbonyl group and ESP distributions of the three COFs are approximate because of the similar structures in which TpPa-COF is flatter based on the superior integrity of π-conjugation.

To further expand the application of TpBD-COF photocatalysis, a wide variety of amines with different substitutes were applied to the standard reaction protocol. Clearly, almost all primary amines could be adequately oxidized to corresponding imines with gratifying selectivities by TpBD-COF photocatalysis (Table 1). Some of the patterns could be summarized by contrasting to the photocatalytic activity of the different amines. Notably, the electronic effect of the substitutes is critical during the selective oxidation of amines. With the electron-donating *para* substitutes of benzyl amines, the higher conversion of the photocatalytic oxidation was reached compared with benzylamine (Table 1, entries 1 versus 2), whereas that with the electron-withdrawing *para* substitutes were inferior (Table 1, entries 3–5), which was owing to electronic effects of different substituents on the electron density of the benzyl group. In addition, benzyl amines with halogen substitutes further testified the electronic effect manifested as conversion increased with the amplifying electronegativity (Table 1,

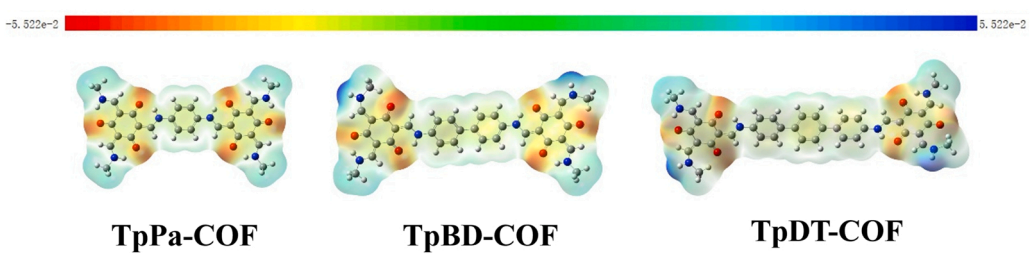

Fig. 8. The ESP surface maps for optimized structures of the three COFs.

Table 1
The aerobic oxidation of primary amines to imines by TpBD-COF photocatalysis[a].

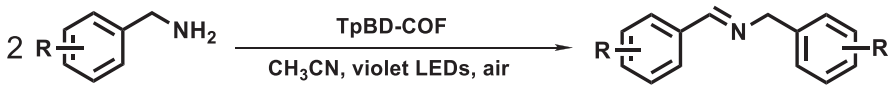

Entry	Substrate	Product	t (h)	Conv. (%)	Sel. (%)
1	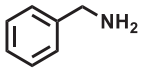	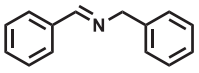	2.7	90	96
2	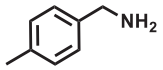	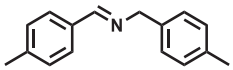	2.5	90	98
3	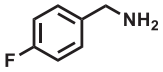	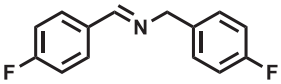	3.1	94	94
4	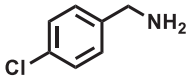	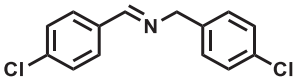	3.5	96	99
5	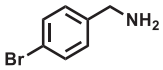	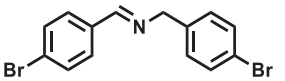	4.0	94	99
6	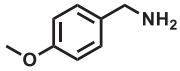	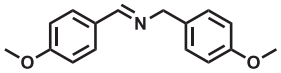	2.5	96	99
7	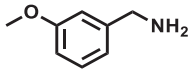	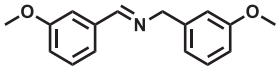	3.1	95	99
8	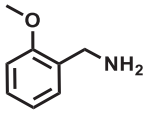	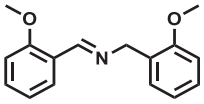	2.7	90	99
9	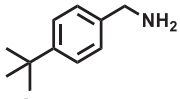	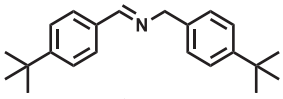	2.9	94	99
10	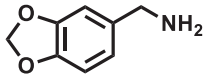	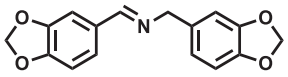	2.5	94	99
11	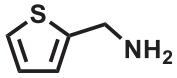	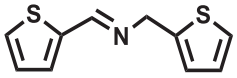	2.5	46	82
12	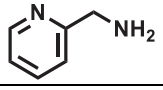	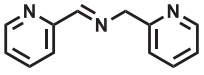	2.5	97	99

[a] Reaction conditions: primary amine (0.3 mmol), TpBD-COF (5 mg), violet LEDs, air (1 atm), CH_3CN (1 mL).

entries 3–5). Besides, the steric effect of of the substitutes also has a significant effect on the selective oxidation of amines. When changing the position of the methoxy substitute (Table 1, entries 6–8), the conversions were slightly different according to the order of *para* > *ortho* > *meta* isomer. The *tert*-butylbenzylamine (Table 1, entry 9) had almost no difference to the conversion of benzylamine for the combined electronic and steric effect. Interestingly, piperonylamine (Table 1, entry 10) and the amines bearing heteroatom N and S (Table 1, entries 11 and 12) were also applicable to the standard reaction protocol.

Subsequently, several secondary amines were applied to further verify the universality of TpBD-COF photocatalysis (Table 2). Secondary amines could be transformed into corresponding imines (Table 2, entries 1–7). But selectivities for the oxidation of secondary benzyl amines were inferior to that of oxidation of primary amines (Table 2, entries 1–4). The results further demonstrate the universality of TpBD-COF photocatalysis in the aerobic oxidation of various amines to imines.

3.3. Mechanistic investigation of TpBD-COF photocatalysis

Based on the above results, it is clear that TpBD-COF is genuinely applicable towards the selective oxidation of amines. Then the reaction mechanism of TpBD-COF photocatalysis was vigorously elucidated. Previous work suggests that both electron transfer and energy transfer pathways are instrumental for the selective oxidation of amines irradiated by visible light [71]. Here, a series of experiments were performed for clarifying the generated reactive oxygen species (ROS) in the selective oxidation of benzylamine. As shown in Table 3, the conversion of benzylamine was 78% under the standard reaction conditions (Table 3, entry 1). Filled with N_2, the conversion of benzylamine almost didn't exist, illustrating that O_2 took up the indispensable position as the terminal oxidant (Table 3, entry 2). The addition of $AgNO_3$ as e^- scavenger lowered the conversion of benzylamine due to impeding the reduction of O_2 to $O_2^{\bullet-}$. Thus $O_2^{\bullet-}$ should play a significant part in the oxidation of benzylamine (Table 3, entry 3). When CD_3CN was added as the solvent of the reaction, the existence time of singlet oxygen ($^1O_2$) could be prolonged. On the contrary, the conversion of benzylamine did not rise (Table 3, entry 4), reflecting that $^1O_2$ did not take part in the reaction process. Besides, NaN_3 is the efficient scavenger for capturing $^1O_2$, but the conversion of benzylamine did little change (Table 3, entry 5), further indicating that $^1O_2$ did not contribute to the oxidation of benzylamine. On the whole, the primary ROS of TpBD-COF photocatalysis is $O_2^{\bullet-}$ for the selective oxidation of benzylamine.

Besides, in situ electron paramagnetic resonance (EPR) spectroscopy was used to further validate the generated active species by spin

Table 2
The aerobic oxidation of secondary amines to imines by TpBD-COF photocatalysis[a].

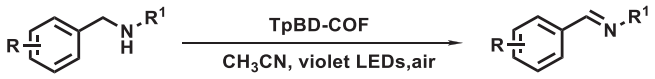

Entry	Substrate	Product	Conv. (%)	Sel. (%)
1	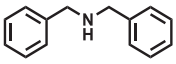	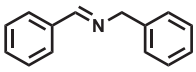	65	74
2	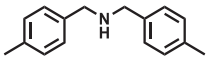	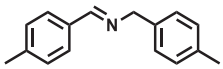	93	51
3	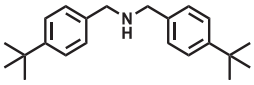	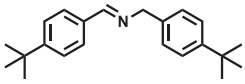	81	62
4	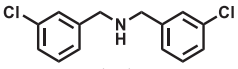	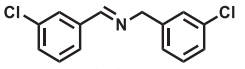	33	88
5	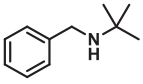	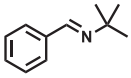	66	99
6	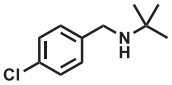	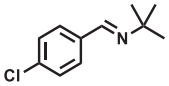	66	99
7	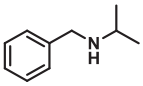	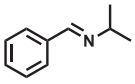	51	64

[a] Reaction conditions: secondary amines (0.15 mmol), TpBD-COF (5 mg), violet LEDs, air (1 atm), CH_3CN (1 mL), 2.5 h.

Table 3
Results of ROS quenching for the aerobic oxidation of benzylamine[a].

Entry	Quencher	Equiv.	Role	Conv. (%)	Sel. (%)
1	None	–	–	78	99
2	N_2	–	O_2 replacement	0	–
3	$AgNO_3$	1	e^- scavenger	0	–
4	CD_3CN	–	$^1O_2$ maintainer	70	92
5	NaN_3	–	$^1O_2$ scavenger	63	99

[a] Reaction conditions: benzylamine (0.3 mmol), TpBD-COF (5 mg), violet LEDs, air (1 atm), CH_3CN (1 mL), 2 h.

trapping. As plotted in Fig. 9a, the continuously increased signal assigned to electron (e^-) transfer from HOMO to LUMO was observed over TpBD-COF irradiated by violet light. A weaker signal was observed as the introduction of O_2 for the reason that e^- combined with O_2. With the addition of 5,5-dimethyl-pyrroline-*N*-oxide (DMPO) (Fig. 9b), a spin trap of $O_2^{\bullet-}$, the remarkably enhanced signal as the increased time of irradiation confirmed the formation of $O_2^{\bullet-}$ during the selective oxidation of benzylamine.

Gradually, a proposed mechanism for the aerobic oxidation of benzylamine by TpBD-COF photocatalysis is illustrated in Fig. 10. Firstly, TpBD-COF acts as transfer channels prompting the separation of electron–hole pairs (e^-–h^+) irradiated by violet light. Then e^- migrates from the HOMO of the TpBD-COF to its LUMO, reducing O_2 to $O_2^{\bullet-}$. Secondly, h^+ drifts to the surface of TpBD-COF, rapidly oxidizing benzylamine to benzylamine radical cation. Subsequently, the formed $O_2^{\bullet-}$ reacts with the benzylamine radical cation to engender benzaldimine. Eventually, the desired product *N*-benzylbenzaldimine is delivered by condensing benzaldimine and benzylamine.

4. Conclusions

In summary, three β-ketoenamine COFs with different linker lengths have been built successfully by changing the building blocks, which have large specific surface area and high crystallinity. The relationship has been established between the linker lengths of the three COFs and the photocatalytic activity for the selective oxidation of benzylamine. The increase in linker lengths from 1,4-benzenediamine to 4,4′-biphenyldiamine can contribute to extending π-conjugation. In contrast, the backbone tends to distort, and the planarity is liable to weaken when linker lengths continue to increase from 4,4′-biphenyldiamine to 4,4″-*p*-

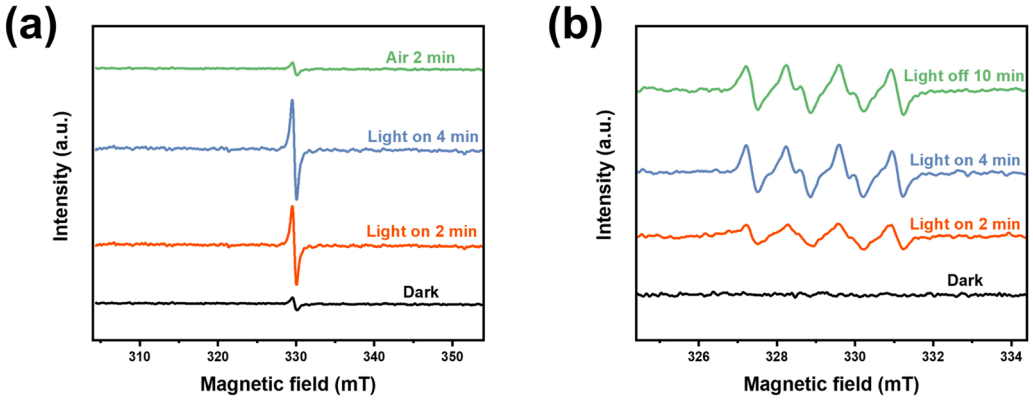

Fig. 9. The EPR spectra of (a) e^- and (b) spin trapping of $O_2^{\bullet-}$ with DMPO during the aerobic oxidation of benzylamine by TpBD-COF photocatalysis.

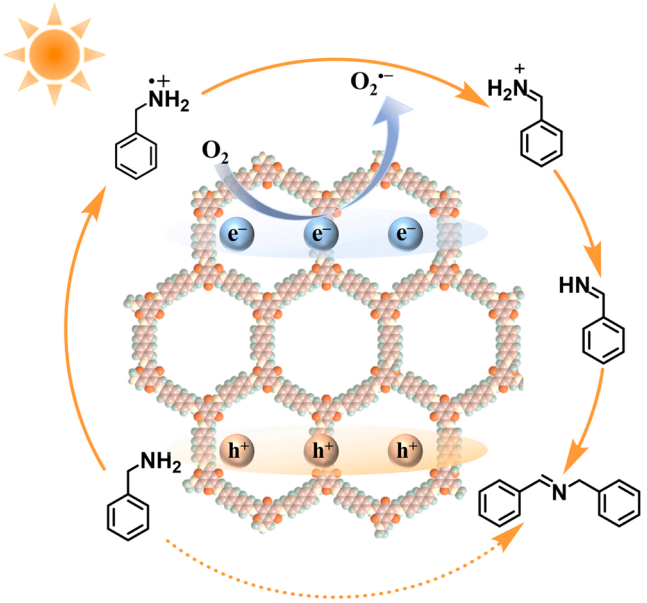

Fig. 10. A proposed mechanism of the aerobic oxidation of benzylamine to *N*-benzylbenzaldimine by TpBD-COF photocatalysis.

terphenyldiamine. Therefore, TpBD-COF with a moderate linker lengths come into being the most suitable redox potentials, thereby enhancing the photocatalytic activity. Compellingly, TpBD-COF exhibited superior photocatalytic conversions to the other two COFs for the selective aerobic oxidation of benzylamine. This work provides a novel dimension for the development and design of more active COF photocatalysts.

CRediT authorship contribution statement

Kanghui Xiong: Investigation, Formal analysis, Writing – original draft; **Yuexin Wang**: Investigation, Formal analysis **Fulin Zhang**: Investigation, Formal analysis; **Xia Li**: Investigation, Formal analysis; **Xianjun Lang**: Conceptualization, Supervision, Writing – review & editing and Funding acquisition.

Declaration of Competing Interest

The authors declare that they have no known competing financial interests or personal relationships that could have appeared to influence the work reported in this paper.

Data availability

Data will be made available on request.

Acknowledgements

This work was funded by the National Natural Science Foundation of China (Grants 22072108 and 21773173).

Appendix A. Supporting information

Supplementary data associated with this article can be found in the online version at doi:10.1016/j.apcatb.2022.122135.

References

[1] T. Zhang, G. Zhang, L. Chen, 2D conjugated covalent organic frameworks: Defined synthesis and tailor-made functions, Acc. Chem. Res. 55 (2022) 795–808, https://doi.org/10.1021/acs.accounts.1c00693.

[2] H. Wang, H. Wang, Z.W. Wang, L. Tang, G.M. Zeng, P. Xu, M. Chen, T. Xiong, C. Y. Zhou, X.Y. Li, D.N. Huang, Y. Zhu, Z.X. Wang, J.W. Tang, Covalent organic framework photocatalysts: Structures and applications, Chem. Soc. Rev. 49 (2020) 4135–4165, https://doi.org/10.1039/d0cs00278j.

[3] J. Yang, F.Y. Kang, X. Wang, Q.C. Zhang, Design strategies for improving the crystallinity of covalent organic frameworks and conjugated polymers: A review, Mater. Horiz. 9 (2022) 121–146, https://doi.org/10.1039/d1mh00809a.

[4] X.Y. Guan, H. Li, Y.C. Ma, M. Xue, Q.R. Fang, Y.S. Yan, V. Valtchev, S.L. Qiu, Chemically stable polyarylether-based covalent organic frameworks, Nat. Chem. 11 (2019) 587–594, https://doi.org/10.1038/s41557-019-0238-5.

[5] Q. Yang, M.L. Luo, K.W. Liu, H.M. Cao, H.J. Yan, Covalent organic frameworks for photocatalytic applications, Appl. Catal. B: Environ. 276 (2020), 119174, https://doi.org/10.1016/j.apcatb.2020.119174.

[6] L.P. Guo, J. Zhang, Q. Huang, W. Zhou, S.B. Jin, Progress in synthesis of highly crystalline covalent organic frameworks and their crystallinity enhancement strategies, Chin. Chem. Lett. 33 (2022) 2856–2866, https://doi.org/10.1016/j.cclet.2022.02.065.

[7] T. Sun, J. Xie, W. Guo, D.S. Li, Q.C. Zhang, Covalent–organic frameworks: Advanced organic electrode materials for rechargeable batteries, Adv. Energy Mater. 10 (2020), 1904199, https://doi.org/10.1002/aenm.201904199.

[8] S. Cao, B. Li, R.M. Zhu, H. Pang, Design and synthesis of covalent organic frameworks towards energy and environment fields, Chem. Eng. J. 355 (2019) 602–623, https://doi.org/10.1016/j.cej.2018.08.184.

[9] S. Wang, Q.Y. Wang, P.P. Shao, Y.Z. Han, X. Gao, L. Ma, S. Yuan, X.J. Ma, J. W. Zhou, X. Feng, B. Wang, Exfoliation of covalent organic frameworks into few-layer redox-active nanosheets as cathode materials for lithium-ion batteries, J. Am. Chem. Soc. 139 (2017) 4258–4261, https://doi.org/10.1021/jacs.7b02648.

[10] Z.F. Wang, S.N. Zhang, Y. Chen, Z.J. Zhang, S.Q. Ma, Covalent organic frameworks for separation applications, Chem. Soc. Rev. 49 (2020) 708–735, https://doi.org/10.1039/c9cs00827f.

[11] H.W. Fan, A. Mundstock, A. Feldhoff, A. Knebel, J.H. Gu, H. Meng, J. Caro, Covalent organic framework–covalent organic framework bilayer membranes for highly selective gas separation, J. Am. Chem. Soc. 140 (2018) 10094–10098, https://doi.org/10.1021/jacs.8b05136.

[12] H.L. Qian, C.X. Yang, W.L. Wang, C. Yang, X.P. Yan, Advances in covalent organic frameworks in separation science, J. Chromatogr. A 1542 (2018) 1–18, https://doi.org/10.1016/j.chroma.2018.02.023.

[13] Y.P. Ying, M.M. Tong, S.C. Ning, S.K. Ravi, S.B. Peh, S.C. Tan, S.J. Pennycook, D. Zhao, Ultrathin two-dimensional membranes assembled by ionic covalent organic nanosheets with reduced apertures for gas separation, J. Am. Chem. Soc. 142 (2020) 4472–4480, https://doi.org/10.1021/jacs.9b13825.

[14] S.H. Xiong, L. Li, L. Dong, J.T. Tang, G.P. Yu, C.Y. Pan, Covalent-organic frameworks (COFs)-based membranes for CO_2 separation, J. CO_2 Util. 41 (2020), 101224, https://doi.org/10.1016/j.jcou.2020.101224.

[15] N. Keller, T. Bein, Optoelectronic processes in covalent organic frameworks, Chem. Soc. Rev. 50 (2021) 1813–1845, https://doi.org/10.1039/d0cs00793e.

[16] Y.Z. Yang, K. Börjesson, Electroactive covalent organic frameworks: A new choice for organic electronics, Trends Chem. 4 (2022) 60–75, https://doi.org/10.1016/j.trechm.2021.10.007.

[17] X.Y. Wang, L.J. Chen, S.Y. Chong, M.A. Little, Y.Z. Wu, W.H. Zhu, R. Clowes, Y. Yan, M.A. Zwijnenburg, R.S. Sprick, A.I. Cooper, Sulfone-containing covalent organic frameworks for photocatalytic hydrogen evolution from water, Nat. Chem. 10 (2018) 1180–1189, https://doi.org/10.1038/s41557-018-0141-5.

[18] W.B. Liu, X.K. Li, C.M. Wang, H.H. Pan, W.P. Liu, K. Wang, Q.D. Zeng, R.M. Wang, J.Z. Jiang, A scalable general synthetic approach toward ultrathin imine-linked two-dimensional covalent organic framework nanosheets for photocatalytic CO_2 reduction, J. Am. Chem. Soc. 141 (2019) 17431–17440, https://doi.org/10.1021/jacs.9b09502.

[19] C.S. Diercks, S. Lin, N. Komienko, E.A. Kapustin, E.M. Nichols, C.H. Zhu, Y.B. Zhao, C.J. Chang, O.M. Yaghi, Reticular electronic tuning of porphyrin active sites in covalent organic frameworks for electrocatalytic carbon dioxide reduction, J. Am. Chem. Soc. 140 (2018) 1116–1122, https://doi.org/10.1021/jacs.7b11940.

[20] P.F. Wei, M.Z. Qi, Z.P. Wang, S.Y. Ding, W. Yu, Q. Liu, L.K. Wang, H.Z. Wang, W. K. An, W. Wang, Benzoxazole-linked ultrastable covalent organic frameworks for photocatalysis, J. Am. Chem. Soc. 140 (2018) 4623–4631, https://doi.org/10.1021/jacs.8b00571.

[21] Y.F. Zhi, Z.R. Wang, H.L. Zhang, Q.C. Zhang, Recent progress in metal-free covalent organic frameworks as heterogeneous catalysts, Small 16 (2020), 2001070, https://doi.org/10.1002/smll.202001070.

[22] S.Z. Yang, W.H. Hu, X. Zhang, P.L. He, B. Pattengale, C.M. Liu, M. Cendejas, I. Hermans, X.Y. Zhang, J. Zhang, J.E. Huang, 2D covalent organic frameworks as intrinsic photocatalysts for visible light-driven CO_2 reduction, J. Am. Chem. Soc. 140 (2018) 14614–14618, https://doi.org/10.1021/jacs.8b09705.

[23] J.H. You, Y. Zhao, L. Wang, W.T. Bao, Recent developments in the photocatalytic applications of covalent organic frameworks: A review, J. Cleaner Prod. 291 (2021), 125822, https://doi.org/10.1016/j.jclepro.2021.125822.

[24] M. Lu, M. Zhang, J. Liu, Y.F. Chen, J.P. Liao, M.Y. Yang, Y.P. Cai, S.L. Li, Y.Q. Lan, Covalent organic framework based functional materials: Important catalysts for efficient CO_2 utilization, Angew. Chem. Int. Ed. 61 (2022), e202200003, https://doi.org/10.1002/anie.202200003.

[25] W.G. Tu, Y. Xu, S.M. Yin, R. Xu, Rational design of catalytic centers in crystalline frameworks, Adv. Mater. 30 (2018), 1707582, https://doi.org/10.1002/adma.201707582.

[26] W. Li, X. Ding, B.Q. Yu, H.L. Wang, Z. Gao, X.X. Wang, X.L. Liu, K. Wang, J. Z. Jiang, Tuning molecular chromophores of isoreticular covalent organic

frameworks for visible light-induced hydrogen generation, Adv. Funct. Mater. 32 (2022), 2207394, https://doi.org/10.1002/adfm.202207394.
[27] F.L. Liu, Y.Y. He, X.P. Liu, Z. Wang, H.L. Liu, X. Zhu, C.C. Hou, Y.X. Weng, Q. F. Zhang, Y. Chen, Regulating excitonic effects in covalent organic frameworks to promote free charge carrier generation, ACS Catal. (2022) 9494–9502, https://doi.org/10.1021/acscatal.2c02173.
[28] K. Lei, D. Wang, L.Q. Ye, M.P. Kou, Y. Deng, Z.Y. Ma, L. Wang, Y. Kong, A metal-free donor–acceptor covalent organic framework photocatalyst for visible-light-driven reduction of CO_2 with H_2O, ChemSusChem 13 (2020) 1725–1729, https://doi.org/10.1002/cssc.201903545.
[29] P. Shang, X. Yan, Y. Li, J. Liu, G. Zhang, L. Chen, Heterogeneous photocatalytic borylation of aryl iodides mediated by isoreticular 2D covalent organic frameworks, Chin. Chem. Lett. (2023), https://doi.org/10.1016/j.cclet.2022.06.007.
[30] Y. Li, X.Y. Song, G. Zhang, L. Wang, Y. Liu, W.H. Chen, L. Chen, 2D covalent organic frameworks toward efficient photocatalytic hydrogen evolution, ChemSusChem 15 (2022), e202200901, https://doi.org/10.1002/cssc.202200901.
[31] F. Beuerle, B. Gole, Covalent organic frameworks and cage compounds: Design and applications of polymeric and discrete organic scaffolds, Angew. Chem. Int. Ed. 57 (2018) 4850–4878, https://doi.org/10.1002/anie.201710190.
[32] W.W. Zhang, L.J. Chen, S. Dai, C.X. Zhao, C. Ma, L. Wei, M.H. Zhu, S.Y. Chong, H. F. Yang, L.J. Liu, Y. Bai, M.J. Yu, Y.J. Xu, X.W. Zhu, Q. Zhu, S.H. An, R.S. Sprick, M. A. Little, X.F. Wu, S. Jiang, Y.Z. Wu, Y.B. Zhang, H. Tian, W.H. Zhu, A.I. Cooper, Reconstructed covalent organic frameworks, Nature 604 (2022) 72–79, https://doi.org/10.1038/s41586-022-04443-4.
[33] S.M. Chai, X.W. Chen, X.R. Zhang, Y.X. Fang, R.S. Sprick, X. Chen, Rational design of covalent organic frameworks for efficient photocatalytic hydrogen peroxide production, Environ. Sci. Nano 9 (2022) 2464–2469, https://doi.org/10.1039/d2en00135g.
[34] W.B. Chen, L. Wang, D.Z. Mo, F. He, Z.L. Wen, X.J. Wu, H.X. Xu, L. Chen, Modulating benzothiadiazole-based covalent organic frameworks via halogenation for enhanced photocatalytic water splitting, Angew. Chem. Int. Ed. 59 (2020) 16902–16909, https://doi.org/10.1002/anie.202006925.
[35] Y.Y. Wan, L. Wang, H.X. Xu, X.J. Wu, J.L. Yang, A simple molecular design strategy for two-dimensional covalent organic framework capable of visible-light-driven water splitting, J. Am. Chem. Soc. 142 (2020) 4508–4516, https://doi.org/10.1021/jacs.0c00564.
[36] F.Y. Liu, Z.Y. Ma, Y.C. Deng, M. Wang, P. Zhou, W. Liu, S.J. Guo, M.P. Tong, D. Ma, Tunable covalent organic frameworks with different heterocyclic nitrogen locations for efficient Cr(VI) reduction, *Escherichia coli* disinfection, and paracetamol degradation under visible-light irradiation, Environ. Sci. Technol. 55 (2021) 5371–5381, https://doi.org/10.1021/acs.est.0c07857.
[37] S.S. Tao, D.L. Jiang, Covalent organic frameworks for energy conversions: Current status, challenges, and perspectives, CCS Chem. 3 (2021) 2003–2024, https://doi.org/10.31635/ccschem.020.202000491.
[38] Y.X. Wang, C.J. Kang, Z.Q. Zhang, A.K. Usadi, D.C. Calabro, L.S. Baugh, Y.D. Yuan, D. Zhao, Evaluation of Schiff-base covalent organic frameworks for CO_2 capture: Structure–performance relationships, stability, and performance under wet conditions, ACS Sustainable Chem. Eng. 10 (2022) 332–341, https://doi.org/10.1021/acssuschemeng.1c06318.
[39] B.P. Biswal, S. Chandra, S. Kandambeth, B. Lukose, T. Heine, R. Banerjeet, Mechanochemical synthesis of chemically stable isoreticular covalent organic frameworks, J. Am. Chem. Soc. 135 (2013) 5328–5331, https://doi.org/10.1021/ja4017842.
[40] C.R. DeBlase, K.E. Silberstein, T.T. Truong, H.D. Abruna, W.R. Dichtel, β-Ketoenamine-linked covalent organic frameworks capable of pseudocapacitive energy storage, J. Am. Chem. Soc. 135 (2013) 16821–16824, https://doi.org/10.1021/ja409421d.
[41] L.T. Wang, L.L. Zhang, B.Z. Lin, Y.Z. Zheng, J.L. Chen, Y. Zheng, B.F. Gao, J. L. Long, Y.L. Chen, Activation of carbonyl oxygen sites in β-ketoenamine-linked covalent organic frameworks via cyano conjugation for efficient photocatalytic hydrogen evolution, Small 17 (2021), 2101017, https://doi.org/10.1002/smll.202101017.
[42] M.P. Kou, Y.Y. Wang, Y.X. Xu, L.Q. Ye, Y.P. Huang, B.H. Jia, H. Li, J.Q. Ren, Y. Deng, J.H. Chen, Y. Zhou, K. Lei, L. Wang, W. Liu, H.W. Huang, T.Y. Ma, Molecularly engineered covalent organic frameworks for hydrogen peroxide photosynthesis, Angew. Chem. Int. Ed. 61 (2022), e202200413, https://doi.org/10.1002/anie.202200413.
[43] L. Xu, J. Xu, B.T. Shan, X.L. Wang, C.J. Gao, TpPa-2-incorporated mixed matrix membranes for efficient water purification, J. Membr. Sci. 526 (2017) 355–366, https://doi.org/10.1016/j.memsci.2016.12.039.
[44] M. Lu, Q. Li, J. Liu, F.M. Zhang, L. Zhang, J.L. Wang, Z.H. Kang, Y.Q. Lan, Installing earth-abundant metal active centers to covalent organic frameworks for efficient heterogeneous photocatalytic CO_2 reduction, Appl. Catal. B: Environ. 254 (2019) 624–633, https://doi.org/10.1016/j.apcatb.2019.05.033.
[45] S. Chandra, S. Kandambeth, B.P. Biswal, B. Lukose, S.M. Kunjir, M. Chaudhary, R. Babarao, T. Heine, R. Banerjee, Chemically stable multilayered covalent organic nanosheets from covalent organic frameworks via mechanical delamination, J. Am. Chem. Soc. 135 (2013) 17853–17861, https://doi.org/10.1021/ja408121p.
[46] P.Y. Dong, Y. Wang, A.C.J. Zhang, T. Cheng, X.G. Xi, J.L. Zhang, Platinum single atoms anchored on a covalent organic framework: Boosting active sites for photocatalytic hydrogen evolution, ACS Catal. 11 (2021) 13266–13279, https://doi.org/10.1021/acscatal.1c03441.
[47] P. Pachfule, A. Acharjya, J. Roeser, T. Langenhahn, M. Schwarze, R. Schomäcker, A. Thomas, J. Schmidt, Diacetylene functionalized covalent organic framework (COF) for photocatalytic hydrogen generation, J. Am. Chem. Soc. 140 (2018) 1423–1427, https://doi.org/10.1021/jacs.7b11255.
[48] B.P. Biswal, H.A. Vignolo-González, T. Banerjee, L. Grunenberg, G. Savasci, K. Gottschling, J. Nuss, C. Ochsenfeld, B.V. Lotsch, Sustained solar H_2 evolution from a thiazolo[5,4-*d*]thiazole-bridged covalent organic framework and nickel-thiolate cluster in water, J. Am. Chem. Soc. 141 (2019) 11082–11092, https://doi.org/10.1021/jacs.9b03243.
[49] L. Wang, J.X. Mao, G.F. Huang, Y. Zhang, J.W. Huang, H.D. She, C.L. Liu, H. Liu, Q. Z. Wang, Configuration of hetero-framework via integrating MOF and triazine-containing COF for charge-transfer promotion in photocatalytic CO_2 reduction, Chem. Eng. J. 446 (2022), 137011, https://doi.org/10.1016/j.cej.2022.137011.
[50] L.Y. Yin, Y.N. Zhao, Y.M. Xing, H.Q. Tan, Z.L. Lang, W.K. Ho, Y.H. Wang, Y.G. Li, Structure-property relationship in β-keto-enamine-based covalent organic frameworks for highly efficient photocatalytic hydrogen production, Chem. Eng. J. 419 (2021), 129984, https://doi.org/10.1016/j.cej.2021.129984.
[51] S.X. Yang, T.C. Li, Y. Cheng, W.W. Fan, L.J. Wang, Y.X. Liu, L.C. Bian, C.H. Zhou, L. Y. Zheng, Q.E. Cao, Covalent organic framework isomers for photoenhanced gold recovery from E-waste with high efficiency and selectivity, ACS Sustainable Chem. Eng. 10 (2022) 9719–9731, https://doi.org/10.1021/acssuschemeng.2c00285.
[52] W. Wang, S.B. Deng, L. Ren, D.Y. Li, W.J. Wang, M. Vakili, B. Wang, J. Huang, Y. J. Wang, G. Yu, Stable covalent organic frameworks as efficient adsorbents for high and selective removal of an aryl-organophosphorus flame retardant from water, ACS Appl. Mater. Interfaces 10 (2018) 30265–30272, https://doi.org/10.1021/acsami.8b06229.
[53] S. Kandambeth, A. Mallick, B. Lukose, M.V. Mane, T. Heine, R. Banerjee, Construction of crystalline 2D covalent organic frameworks with remarkable chemical (acid/base) stability via a combined reversible and irreversible route, J. Am. Chem. Soc. 134 (2012) 19524–19527, https://doi.org/10.1021/ja308278w.
[54] T. Zhou, L. Wang, X.Y. Huang, J. Unruangsri, H.L. Zhang, R. Wang, Q.L. Song, Q. Y. Yang, W.H. Li, C.C. Wang, K. Takahashi, H.X. Xu, J. Guo, PEG-stabilized coaxial stacking of two-dimensional covalent organic frameworks for enhanced photocatalytic hydrogen evolution, Nat. Commun. 12 (2021) 3934, https://doi.org/10.1038/s41467-021-24179-5.
[55] J.L. Li, Z.W. Zhang, J. Jia, X.M. Liu, Covalent organic frameworks for photocatalytic organic transformation, Chem. Res. Chin. Univ. 38 (2022) 275–289, https://doi.org/10.1007/s40242-022-1434-1.
[56] Y.Z. Cheng, W.Y. Ji, X.X. Wu, X.S. Ding, X.F. Liu, B.H. Han, Persistent radical cation sp^2 carbon-covalent organic framework for photocatalytic oxidative organic transformations, Appl. Catal. B: Environ. 306 (2022), 121110, https://doi.org/10.1016/j.apcatb.2022.121110.
[57] Z.P. Li, J.A. Wang, S. Ma, Z.W. Zhang, Y.F. Zhi, F.C. Zhang, H. Xia, G. Henkelman, X.M. Liu, 2D covalent organic frameworks for photosynthesis of α-trifluoromethylated ketones from aromatic alkenes, Appl. Catal. B: Environ. 310 (2022), 121335, https://doi.org/10.1016/j.apcatb.2022.121335.
[58] J. Zhou, X.M. Ma, Y.X. Wang, X. Li, X.J. Lang, Visible light-initiated aerobic oxidation of amines to imines over TiO_2 microspheres with $TEMPO^+PF_6^-$, Sustainable Energy Fuels 6 (2022) 894–902, https://doi.org/10.1039/d1se01829a.
[59] Z.X. Sun, K. Sun, M.L. Gao, O. Metin, H.L. Jiang, Optimizing Pt electronic states through formation of a Schottky junction on non-reducible metal–organic frameworks for enhanced photocatalysis, Angew. Chem. Int. Ed. 61 (2022), e202206108, https://doi.org/10.1002/anie.202206108.
[60] H.T. Wang, J.N. Yu, S. Wei, M.M. Lin, Y.J. Song, L. Wu, Surface coordination enhanced visible-light photocatalytic coupling of benzylamine to N-benzylidene benzylamine over the Pd/NH_2-MIL-125(Ti) nanosheets, Chem. Eng. J. 441 (2022), 136020, https://doi.org/10.1016/j.cej.2022.136020.
[61] X. Li, F.L. Zhang, Y.X. Wang, K.H. Xiong, X.J. Lang, Extending the 2D conjugated microporous polymers linked by thiazolo[5,4-*d*]thiazole for green light-driven selective aerobic oxidation of amines, J. Mater. Chem. A 10 (2022) 14965–14975, https://doi.org/10.1039/d2ta02603a.
[62] H.J. He, X. Fang, D. Zhai, W. Zhou, Y.M. Li, W.L. Zhao, C.C. Liu, Z. Li, W.Q. Deng, A porphyrin-based covalent organic framework for metal-free photocatalytic aerobic oxidative coupling of amines, Chem. Eur. J. 27 (2021) 14390–14395, https://doi.org/10.1002/chem.202102239.
[63] W.Q. Li, X.F. Huang, T.W. Zeng, Y.A. Liu, W.B. Hu, H. Yang, Y.B. Zhang, K. Wen, Thiazolo[5,4-*d*]thiazole-based donor–acceptor covalent organic framework for sunlight-driven hydrogen evolution, Angew. Chem. Int. Ed. 60 (2021) 1869–1874, https://doi.org/10.1016/j.chempr.2022.07.016.
[64] J.L. Shi, R.F. Chen, H.M. Hao, C. Wang, X.J. Lang, 2D sp^2 carbon-conjugated porphyrin covalent organic framework for cooperative photocatalysis with TEMPO, Angew. Chem. Int. Ed. 59 (2020) 9088–9093, https://doi.org/10.1002/anie.202000723.
[65] S. Li, L. Li, Y.J. Li, L. Dai, C.X. Liu, Y.Z. Liu, J.N. Li, J.N. Lv, P.F. Li, B. Wang, Fully conjugated donor–acceptor covalent organic frameworks for photocatalytic oxidative amine coupling and thioamide cyclization, ACS Catal. 10 (2020) 8717–8726, https://doi.org/10.1021/acscatal.0c01242.
[66] Z.Y. Wu, X.B. Huang, X.J. Li, G.T. Hai, B.Z. Li, G. Wang, Covalent-organic frameworks with keto-enol tautomerism for efficient photocatalytic oxidative coupling of amines to imines under visible light, Sci. China Chem. 64 (2021) 2169–2179, https://doi.org/10.1007/s11426-021-1088-2.
[67] X. Li, S.X. Yang, F.L. Zhang, L.Y. Zheng, X.J. Lang, Facile synthesis of 2D covalent organic frameworks for cooperative photocatalysis with TEMPO: The selective aerobic oxidation of benzyl amines, Appl. Catal. B: Environ. 303 (2022), 120846, https://doi.org/10.1016/j.apcatb.2021.120846.
[68] F.L. Zhang, X. Li, X.Y. Dong, H.M. Hao, X.J. Lang, Thiazolo[5,4-*d*]thiazole-based covalent organic framework microspheres for blue light photocatalytic selective

oxidation of amines with O_2, Chin. J. Catal. 43 (2022) 2395–2404, https://doi.org/10.1016/S1872-2067(22)64127-5.

[69] P.L.A. Popelier, P.I. Maxwell, J.C.R. Thacker, I. Alkorta, A relative energy gradient (REG) study of the planar and perpendicular torsional energy barriers in biphenyl, Theor. Chem. Acc. 138 (2019) 1–16, https://doi.org/10.1007/s00214-018-2383-0.

[70] N. Keller, M. Calik, D. Sharapa, H.R. Soni, P.M. Zehetmaier, S. Rager, F. Auras, A. C. Jakowetz, A. Gorling, T. Clark, T. Bein, Enforcing extended porphyrin J-aggregate stacking in covalent organic frameworks, J. Am. Chem. Soc. 140 (2018) 16544–16552, https://doi.org/10.1021/jacs.8b08088.

[71] C.Y. Xu, H. Liu, D.D. Li, J.H. Su, H.L. Jiang, Direct evidence of charge separation in a metal-organic framework: efficient and selective photocatalytic oxidative coupling of amines via charge and energy transfer, Chem. Sci. 9 (2018) 3152–3158, https://doi.org/10.1039/c7sc05296k.